

# Extraction of Neural Activation from Biological Spatio-temporal Imaging Data using Autoregressive Model-based Filtering Technique

Fumikwazu Miwakeichi

Department of Statistical Modeling, the Institute of Statistical Mathematics,  
Department of Statistical Science, the Graduate University for Advanced Studies  
Tachikawa, Tokyo, Japan  
e-mail: miwake1@ism.ac.jp

**Abstract**—Regression and cross-correlation analyses have been widely used to detect neural activation in the dynamic brain imaging data. These analyses require a preliminarily assumed reference function, which reflects temporal changes in neural activation. In other words, only the neural activations, whose temporal patterns resemble to the reference function, can be detected. In cases which reference functions are hardly defined, these analyses are not applicable. In our previous study, we have proposed a method of spatio-temporal filtering to overcome these disadvantages. This method enables us to detect the time and region when and where dynamical state transition according to neural activation arises in repeatedly recorded data (multiple trial data). Moreover, we showed the capability to detect neural activation in single-trial data, such as recording of spontaneous brain activity, using sliding time window.

**Keywords**—Spatio-temporal filtering; Innovation approach; Brain functional imaging; Optical imaging

## I. INTRODUCTION

There have been developed many techniques for biological signal recording e.g., functional magnetic resonance imaging (fMRI) and optical recording, and they enable us to perform detailed investigation of neural activation. However, with the dimensions and size of the data becoming larger and the structure of the data becoming more complicated, a more efficient and automatic method for analysis is required.

One of the widely used methods is based on regression or correlation analysis to detect spatial information of neural activation pattern [1].

For the investigation of microscopic neural activation, an optical imaging technique has been used. This technique offers us the information of temporal transition of membrane potential in excitable tissue [2]-[4]. The structure of optical imaging data is three dimensional: two of them are for space and one is for time. Although the structure of optical imaging data is similar to that of fMRI data, there has been no widely used method for data analysis. Respect to this situation, Oku *et al.* [2], [3] and Okada *et al.* [4] applied time-lagged correlation analysis to optical imaging data to elucidate the mechanism of respiratory rhythm and pattern generation in the rat and frog brainstem. In the studies of rat brainstem [2], [4], they used 4th cervical

spinal cord ventral root (C4VR) output signals that are equivalent to phrenic inspiratory burst activity as the reference function, and found appearances of earlier and simultaneous activities relative to the output signals in the regions of respiratory rhythm generators.

The advantage of regression analysis or cross-correlation analysis is that the significance of the coefficients can be statistically evaluated. Moreover, the test values can be mapped on an anatomical image and it gives spatial information. However, still there have been several problems in these analyses. The regression or correlation analysis evaluates only the morphological resemblance between the time series and the reference function. If there is some activation pattern that does not resemble the reference function, then it cannot be detected. More seriously, in the case that the reference function cannot be defined, the data can hardly be analyzed by these methods.

In the field of time series analysis, innovation approach has been efficiently applied to detect the changes in signal dynamics. The dynamical properties of stationary time series, whose statistical properties, e.g., mean value and variance, do not depend on time, can be identified using mathematical models such as autoregressive (AR) model and autoregressive moving average (ARMA) model [12]. Let us suppose that we prepare two time series; one is used as test time series for model identification, and the other is for filtering with the identified model. If new time series is filtered through the identified model, unpredictable signals remain in residuals. The residuals are called innovations. If the amplitude of innovations of filter output becomes significantly higher than the innovation of test data, the state is detected as a phase transition of dynamics in the system. This approach has been applied in various fields, e.g., plant monitoring system [5]-[9].

In this session, we will review our previous works which applied the innovation approach to optical imaging data attempted to detect biological activation in innovations and introduce methods to evaluate statistical significance of the activation for multiple-trials and single-trial data [10][11].

The methods to detect biological activation is explained in Section II. Section III provides the information about the imaging data which was analysed in this paper. Section IV presents the detected activation using AR model based

filtering method and compare the performance with time-lagged cross-correlation analysis.

## II. METHOD

### A. Time-lagged cross correlation analysis

The time-lagged cross-correlation analysis provides temporal information of the appearance of the signals in the imaging data whose wave forms resemble pre-defined reference function [2]. Suppose  $\eta^v(t)$  is a time series of imaging data for a pixel  $v=(l,m)$  and  $\varphi(t)$  is a pre-defined reference function, the time-lagged cross-correlation can be denoted as

$$R^v(\tau) = \eta^v(t)\varphi(t-\tau) / \sqrt{(\eta^v)^2} \sqrt{\varphi^2}, \quad (1)$$

where  $\tau$  is a relative time lag. The lagged correlation coefficient can be straightforwardly converted to a  $t$ -value. Then time dependent correlation  $t$ -map can be obtained if this procedure is repeated for all pixels. In the case  $\tau = 0$ , it will be ordinary cross-correlation analysis.

### B. Autoregressive(AR) model

There exist many models used for the analysis of time series. The most commonly used model for time series data is the autoregressive (AR) model. The autoregressive process is a difference equation determined by random variables. The most simplest AR model is the first order autoregressive model, written as AR(1), which considers the immediate past value  $\eta(t-1)$  to determine the present value  $\eta(t)$ . An example of AR(1) model is denoted as

$$\eta(t) = 0.8\eta(t-1) + \varepsilon(t), \quad (2)$$

where  $\varepsilon(t)$  is a white noise series with zero mean and variance  $\sigma_\varepsilon^2$ .

An example of second order AR model is denoted as

$$\eta(t) = 1.8596\eta(t-1) - \eta(t-2) + \varepsilon(t). \quad (3)$$

The autoregressive (AR) model for a time series  $\eta(t), t=1, \dots, S$ , can be generalized to the  $p$ -th order AR model, which is defined as a linear combination of the past values with a prediction error  $\varepsilon(t)$  and a constant  $\beta$ ,

$$\eta(t) - \beta = \sum_{i=1}^p \alpha(i)\eta(t-i) + \varepsilon(t), \quad (4)$$

where  $\alpha(i)$  are AR coefficients. The linear dynamic properties of the system can be identified with a parameter vector  $\mathcal{P} = \{\alpha(1), \dots, \alpha(p), \beta, \sigma_\varepsilon^2\}$ , here  $\sigma_\varepsilon^2$  is a variance of  $\varepsilon(t)$ .

In the case of AR(2) model, the relation between AR coefficients and oscillation frequency  $f$  can be denoted as

$$\alpha(1) = 2r \cos\left(2\pi \frac{f}{Fs}\right), \quad \alpha(2) = -r^2, \quad (5)$$

where,  $Fs$  is a sampling frequency and  $r$  is a length of radius in the Gaussian plane which corresponds to attenuation coefficient. For example an oscillation with  $f = 3[\text{Hz}]$ ,  $Fs = 50[\text{Hz}]$  and  $r = 1$  can be realized with (3).

The AR coefficients in (4) can be estimated from actual data by least square method, Yule-Walker method and so on[12]. And the optimal model order  $p$  can be decided by Akaike Information Criterion (AIC)[12][13].

### C. Filtering using AR model

Suppose the AR model is written as,

$$\varepsilon(t) = \eta(t) - \sum_{i=1}^p \alpha(i)\eta(t-i), \quad (6)$$

it can be interpreted as a filter whose input is data and output is prediction error. The prediction error is also called innovation. In the case the frequency for filtering is previously known, the AR coefficients can be adjusted by (5). If the AR coefficients are estimated from actual data, the innovation time series contains the signals which cannot be predict from the vibration characteristic of the data.

The most widely used filtering method is the Fourier-based filtering method to eliminate specific frequency components. Here, the difference between the Fourier-based filtering and AR model based filtering with simulated data. The simulated data was generated by (3) and impulse I was applied as unpredictable signal with AR (2) process,

$$\eta(t) = 1.8596\eta(t-1) - \eta(t-2) + \varepsilon(t) + I. \quad (7)$$

The impulse  $I = 1$  was applied at 3.0[ses] ( $t = 150$ ) and continuously during the period of 4.0-5.0[sec] ( $200 \leq t \leq 250$ ). Fig. 1 (a) and (b) show the simulated time series and output signal from Fourier-based band stop filter (2.5 – 3.5 Hz). Though there can be observed a cusp point at 3[ses] ( $t = 150$ ) in the output signal which correspond to the timing of applied impulse, it is hardly recognized without prior information about the timing. And the onset and offset of continuously applied impulse during 4-5[sec] ( $200 \leq t \leq 250$ ) are not clearly detected. A new AR (2) model was applied to the period of simulated data 0

– 1.0 [sec] and the model was identified with estimating coefficients. And the rest part of the simulated data was filtered through the identified AR (2) model. Fig. 1(c) shows the output signal from the AR (2) model, i.e., innovation times series. Unlike the result from Fourier-based filtering, the amplitude of the innovation time series was steeply increased at the time and the period impulse was applied. This method is called innovation approach.

For the analysis of biological signals, the biological activation can be detected using the AR model based filtering method. However there is possibility that some noise or artifact is also detected. In order to discriminate biological activation and noise or artifact, the amplitude of innovation time series has to be statistically evaluated with repeatedly recorded data. Fig. 2 shows the transition of the amplitude of innovations for all repetitions. The area A is a set of the innovations within the period for model identification and the line B is a set of innovations of filter output at the time  $t'$ . We evaluated the statistical significance of the difference of mean amplitude of the innovations in area A and on line B using standard  $t$ -test.

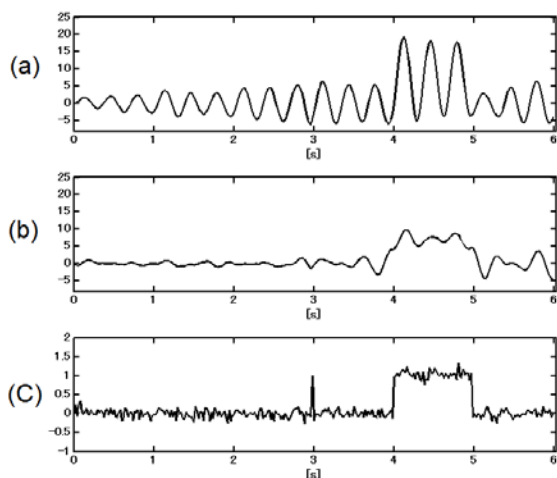


Figure 1. (a) Simulated data with AR(2) process (impulse was applied at 3.0 sec. and continuously during 4.5 – 5.0 sec). (b) Output signal from Fourier-based band stop filter (2.5 Hz – 3.5 Hz) (c) Innovation time series from AR(2) model

### III. BENCHMARK DATA

We selected the same imaging data set from 2 day and 0 day old rats (corresponding to data1 and data2 respectively in this study) that was used in the study of developmental aspects of the respiratory neuronal activation in the rat brainstem [2] in order to evaluate our method by comparing its outputs with those of the time-lagged cross-correlation analysis.

Optical signals were sampled at 50 Hz (20 ms/frame) for data1 and data2. Analog signals of raw and integrated C4VR activities were recorded at 1 kHz for data1 and data2. These analog signals were amplified and digitized, then stored in a hard disk together with optical signals. Analog

signals were window-discriminated to yield Transistor-Transistor Logic (TTL) pulses and used to trigger the optical recording system. Total number of recorded time frames were 1024/256, the recording was started at 768/64 frames before the trigger signal, and repeated 30/34 times for data1/data2, respectively. Among these repetitions, 29 and 27 repetitions, which were contaminated with relatively small artifacts, were selected for data1 and data2, respectively.

Fig. 3 shows the recorded area in the brainstem, which contains two putative rhythm generators those which have been reported as the para-facial respiratory group (pFRG) [12] and the pre-Bötzinger complex (preBötC) [16]. Inspiratory-related respiratory activity was monitored from the C4VR with a suction electrode. The raw nerve signal was amplified, band-pass filtered from 15 Hz to 3 kHz, full-wave rectified, and integrated with a decay time constant of 100ms. This integrated signal was used as the reference function for the cross-correlation analysis. Further experimental condition and preprocessing were explained in [10].

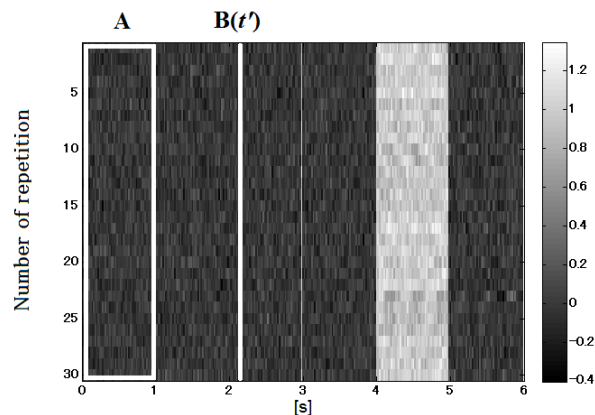


Figure 2. Temporal transition of the amplitude of innovations for all simulated data (30 repetitions). The area A is the set of the innovations within the period of model identification and the line B is the set of the innovations of filter output at the time  $t'$ .

### IV. RESULTS

In the case when imaging data are repeatedly recorded, we obtain multiple time series  $\eta^w(t)$ ,  $t = 1, \dots, S$ , for each pixel ( $w = (l, m, n)$ ,  $l$  and  $m$  are the indices of a pixel,  $n$  is the index of the repetition,  $1 \leq n \leq N$ ) (Fig. 4). The signal from a pixel is contaminated irregular reflection light and scattered light from neighbouring pixels. In order to reduce these contamination, we consider following exogenous type AR model.

Suppose the measurement points of the imaging data are on the two dimensional pixel that are labeled by an index  $v = (l, m)$  and only the influences of nearest neighbor upon each pixel are considered as exogenous inputs, the ARX model will be specialized as

$$\begin{aligned} & \eta^v(t) - \beta^v \\ &= \sum_{i=1}^p \alpha^v(i) \eta^v(t-i) + \sum_{u \in N(v)} \sum_{j=1}^q \delta^u(j) \eta^u(t-j) + \varepsilon^v(t), \end{aligned} \quad (8)$$

where  $N(v)$  is a set of indices of the neighbor pixels to the pixel at  $v = (l, m)$ . Suppose neighbor pixels are restricted to the pixels, which contact with the edge of the pixel at the point  $v$ , a set of indices of neighbor pixels will be

$$N(v) = \{(l+1, m), (l, m-1), (l, m+1), (l-1, m)\}. \quad (9)$$

The ARX model with the restricted neighbor pixels will be referred as Nearest Neighbor Autoregressive model (NNAR) in this paper. The innovations for the pixel at  $v$ ,

$$\begin{aligned} \varepsilon(t)^v &= \eta^v(t) - \hat{\eta}^v(t) \\ &= \eta^v(t) \\ &- \left( \sum_{i=1}^p \alpha^v(i) \eta^v(t-i) + \sum_{u \in N(v)} \sum_{j=1}^q \delta^u(j) \eta^u(t-j) + \beta^v \right) \end{aligned} \quad (10)$$

contain the signals which cannot be predicted by a linear AR process even though the spatial influences from the neighbors are taken into consideration.

Suppose the NNAR model is identified with a limited period  $t_1 \leq t \leq t_2$ , any arbitrary selected other period  $t'_1 \leq t \leq t'_2$  can be filtered through the identified NNAR model. Let the innovations corresponding to the period for the NNAR model identification and for filtering  $\varepsilon^{1,w}(t)$  and  $\varepsilon^{2,w}(t)$ , respectively. The amplitude level of  $\varepsilon^{2,w}(t')$  will increase at the time point  $t'$  when the unpredictable signals arise. Then the statistical significance can be evaluated by comparing the mean value between the innovations at  $t'$ ,  $N^{-1} \sum_{n=1}^N \varepsilon^{2,(l,m,n)}(t')$  and whole innovations

within the period  $t_1 \leq t \leq t_2$ ,  $(N(t_2 - t_1))^{-1} \sum_{t=t_1}^{t_2} \sum_{n=1}^N \varepsilon^{1,(l,m,n)}(t)$

by some statistical test. In this study, we employed standard  $t$ -test for this purpose. By shifting time point  $t'$ , time-dependent  $t$ -values can be computed. Then time-dependent activation  $t$ -map, which shows dynamic state transition, can be obtained by repeating this procedure for all pixels.

This method detects not only biological activation as dynamic state transition but also some artifact inevitably. Some procedure for artifact discrimination has to be considered. There are mainly two types of artifacts. One is stationary oscillatory noise such as those caused by electric power supply (hum noise) and mechanical vibration of measurement system. This sort of artifacts can be identified

by AR-type model, and then  $\varepsilon^{1,w}(t)$  will be close to Gaussian white noise. Therefore the oscillatory noise will not appear in  $\varepsilon^{2,w}(t')$ , because these artifacts consist of predictable signals. The other is caused by non-stationary sporadic noise, and it will appear in  $\varepsilon^{2,w}(t')$  because it cannot be predicted by the identified AR-type model. This sort of artifact can be partly removed from final results such as activation  $t$ -map by setting a threshold for spatial cluster size and/or duration.

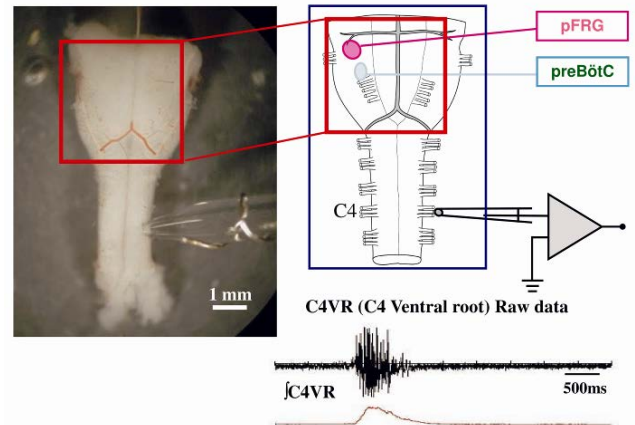


Figure 3. (a) Ventral brainstem area for optical imaging (surrounded by the red square), (b) Schematic representation of anatomical structure of the brainstem and the recorded area, (c) Raw output signal from C4VR, (d) Integrated C4VR output signal.

Background stationary oscillations were identified by a NNAR model on the period sufficiently before or after the respiration onset. In this study four neighboring pixels, which contact with edge of a pixel of interest were employed for the NNAR model for saving the computational cost. The parameters in the NNAR model were estimated using the least square method. Then the rest part of the data was filtered through the identified model and the innovations were estimated. We defined the origin of time axis as the onset of respiratory activity observed in the C4VR signal. The NNAR model was identified on the period sufficiently before the onset of respiratory activity, i.e., from -4.22s to -2.24s (100 time frames). Subsequently, the period from -2.22s to 5.24s (374 time frames) was filtered for the data 1.

In principle, model order of the NNAR model should be optimized according to some criterion, such as Akaike Information Criterion (AIC) [13] for each pixel. However, since it would not be appropriate to individually optimize the model order for a large number of pixels, a common value should be chosen. It is important to choose a sufficiently large value, lest any relevant correlations in the data should be missed. On the other hand, too large model orders may cause over-fitting problems and reduce the reliability of the estimated model parameter values. In this study, the model order for  $p$  and  $q$  in (10) was fixed to the

same values for the simplification of the model. Then, we gradually increased the model order from two and found that stationary oscillations were properly identified and removed from the innovation by NNAR model with  $p = q = 7$ . Therefore, we conclude that for our data a model order of this value represents a good compromise.

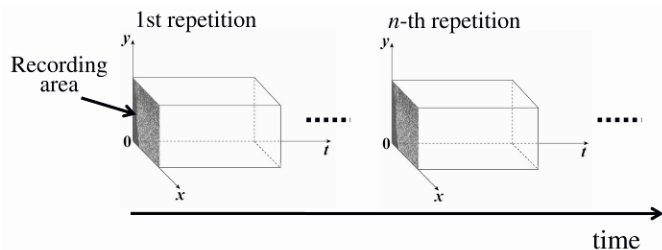


Figure 4. Conceptual representation of the structure of the optical imaging data. The recorded imaging data can be reconstructed with three dimensional data (two dimensional space corresponding to recording area and time axis) for each repetition.

We evaluated the statistical significance of the difference of mean amplitude of the innovations in the period of model identification and filter output by the method mentioned with Fig. 2. This procedure was repeated for all pixels, and then temporal transition of activation  $t$ -map was illustrated. Five representative time frames of activation time map are illustrated as time dependent  $t$ -maps in Fig. 8(c), which shows the area and time at which significant dynamic state transition arises. The activation initiated at the caudal part of pFRG, corresponding to the rostral ventrolateral medulla (RVLM) [14] and [15], and then extended rostrally toward the rostral part of pFRG and caudally toward the preBötC. Subsequently the activation traveled to more caudal structures of the brain. Finally the activation of the high cervical spinal cord reached its maximum (Fig. 5(c) in the time frame at 0.24s) just before the peak of C4VR output signals (Fig. 5(d)). Further, a line from preBötC toward caudal brain structures could be seen in Fig. 5(c) in the time frame at 0.64s. This sequence may correspond to the fact that caudal brain structures such as ventral respiratory group (VRG) contain premotor and motor neurons that relay respiratory outputs to the C3-5 segments of the spinal cord with a certain time delay.

Fig. 5(a) displays activation  $t$ -maps for the raw imaging data instead of the innovations using the procedure described above. Although both images for the imaging data and innovations were thresholded at the same level, significant areas for the imaging data were less than those for the innovations. Further, the propagation from the preBötC toward caudal brain structures could not be detected in activation  $t$ -maps for the raw imaging data.

The results of correlation analysis with averaged imaging data across repetitions is illustrated in Fig. 5(b) as correlation  $t$ -maps. The respiratory related activated areas, such as pFRG and preBötC, were effectively detected. However, the duration of detected activations was shorter

than that of activation  $t$ -maps for the innovations. Besides, the propagation from the preBötC toward caudal brain structures could not be detected.

Data2 did not have enough time frames before the onset of respiratory activation because of the parameter setting for setting recording condition. Therefore the analysis cannot be applied to data2 under the same condition for data1. In order to solve this problem, the NNAR model was identified at the period sufficiently after the onset of respiration, i.e., from 1.98 to 3.96s (100 time frames), and then the period from -1.12 to 1.96s (155 time frames) was filtered. The activation  $t$ -maps for the imaging data and innovations are illustrated in Fig. 6 (a) and (c), respectively. The correlation map is shown in Fig. 6 (b). The analyses yielded similar results to those for data1. Furthermore, the time lag of the activation between preBötC and VRG could be clearly detected in the activation time map for the innovations (Fig. 6 (c) in the time frames of 0s and 0.26s), which was not distinct in the correlation map (Fig. 6 (b)).

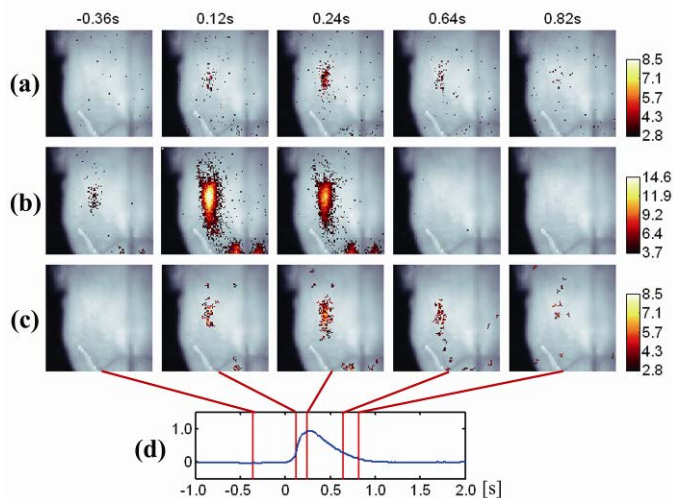


Figure 5. Representative time frames of temporal transition of the activation  $t$ -maps for the imaging data (a) and the innovations (c), and the correlation  $t$ -map with averaged imaging data across repetition (b). The C4VR output signal and time points corresponding to the time frames (d). The  $t$ -maps were thresholded of  $p < 0.05$  (corrected by the False Discovery Rate (FDR)) and a cluster extent of five pixels.

Fig. 2 shows the temporal transition of the amplitude of innovations that was estimated in the simulated data. In the case of the data with single repetition, the line B will consist of only one innovation. Therefore, mean amplitudes of the innovations in the area A and on the line B cannot be statistically evaluated because of the insufficient number of samples. Nevertheless, our method is applicable if the line B is replaced with a time window in order to obtain sufficient number of samples, i.e., innovations, although there is a trade-off with respect to temporal resolution. In this study, we employed a sliding time window  $t' - (w/2) \leq t \leq t' + (w/2)$  ( $w$ : even integer) and the difference of mean values of the innovations within the sliding window  $(t_2 - t_1 + 1)^{-1} \sum_{t=t_1}^{t_2} \varepsilon^{1,v}(t)$  and the period for

NNAR model identification

$$(t_2 - t_1 + 1)^{-1} \sum_{t=t_1}^{t_2} \varepsilon^{1,v}(t) \quad (t_1 \leq t \leq t_2)$$

was evaluated using  $t$ -test. Then, we could obtain time dependent  $t$ -value with sifting time  $t'$ . We empirically selected the width of sliding window at  $w = 30$ . Fig. 7 (b) shows activation  $t$ -maps for five representative time frames from a repetition in data1. The regions of pFRG and preBötC were successively detected and its spatio-temporal distribution pattern is similar to the Fig. 5 (c). Fig. 7 (a) displays activation  $t$ -maps for the raw imaging data instead of the innovations. The square of the detected regions was smaller than the  $t$ -maps from innovation time series.

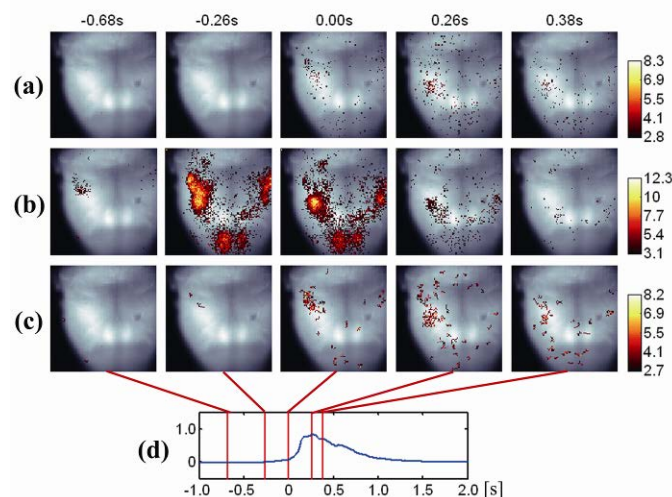


Figure 6. Representative time frames of temporal transition of the activation  $t$ -maps for the imaging data (a) and the innovations (c), and the correlation  $t$ -map with averaged imaging data across repetition (b). The C4VR output signal and time points corresponding to the time frames (d). The  $t$ -maps were thresholded of  $p < 0.05$  (corrected by the False Discovery Rate (FDR)) and a cluster extent of five pixels.

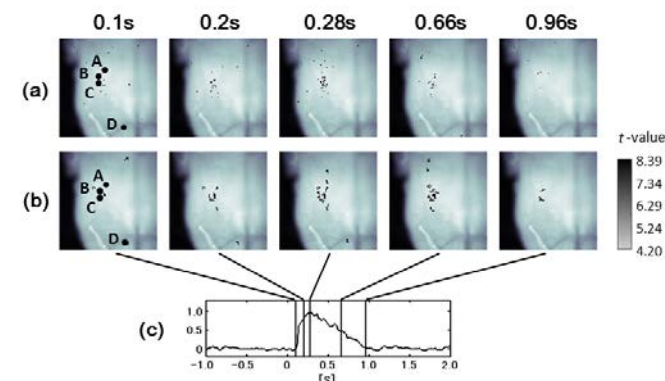


Figure 7. Representative time frames of temporal transition of the activation  $t$ -maps for the imaging data (a) and the innovations (b) The C4VR output signal and time points corresponding to the time frames (c). The  $t$ -maps were thresholded of  $p < 0.05$  (corrected by the False Discovery Rate (FDR)) and a cluster extent of five pixels.

Fig. 8 illustrates temporal fluctuation of the  $t$ -values the point A – D in Fig. 7 (a) and (b) where neural activations were clearly observed in the  $t$ -maps. At the point A, the fluctuations of the  $t$ -values from both raw data and innovations have similar pattern, and exceed the threshold level about 0.28sec later than the onset of inspiration. At the point B and D, only  $t$ -values from the innovation exceed threshold level. The neurons around this region start to activate about 0.1sec earlier and 0.8 sec later than the onset of inspiration respectively. At the point C, the difference of  $t$ -values from the raw data and the innovation is remarkable. There can be seen clear neural activation about 0.1 sec after the onset of inspiration.

V. DISCUSSION

Using the ordinary cross-correlation analysis, which is equivalent to the time-lagged cross-correlation analysis with a restriction  $\tau = 0$ , only one of the two respiratory rhythm generators, the preBötC, was detected with data2. The result can be seen in Fig. 9(b) in the time frame at 0.00s. The reason why the other respiratory rhythm generator was missed is that the activation of pFRG appeared earlier than the onset of the C4VR activity in the reference function. Therefore significant correlation was not found between pFRG and C4VR signals. In this situation, time-lagged cross-correlation analysis gave a solution. Oku, *et al.* [2] applied this method to the optical imaging data and reported an earlier respiratory activation in the pFRG (Fig. 6(b)).

However, there are still several problems in the ordinary or time-lagged cross-correlation analysis. First, it does not consider dynamical properties of time series, but evaluates only morphological resemblance between the two time series. Therefore, only pixels whose temporal activity pattern has a similar shape to the reference function can be detected.

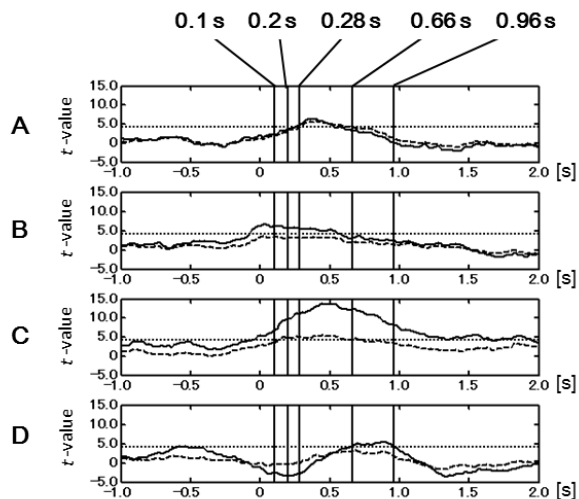


Figure 8. Fluctuation of the  $t$ -values from the raw data (broken line) and the innovations (solid line). The horizontal dotted line indicates threshold level  $t = 4.1950$  ( $p < 0.05$ ) (corrected by the False Discovery Rate (FDR))

Second, it has been applied only to averaged imaging data across the repetition of means. Any method has not been proposed that can be applied to each repetition nor statistically evaluated across the repetition of the measurement. Third, in the case of the time-lagged correlation analysis, the larger the time lag is, the shorter the overlapping length of the two time series becomes. Then, inaccuracy of the analysis will increase with larger time lags. Fourth, the absolute time point of the appearance of activations cannot be investigated by time-lagged cross-correlation analysis. This is because the origin of time axis is defined arbitrarily. Therefore the correlation  $t$ -map of averaged imaging data and activation  $t$ -map for innovations cannot be compared on the common time axis. If the time point corresponding to the peak of C4VR signal is selected as the origin of time frame for the time-lagged cross-correlation, the time point of the onset of activations in the correlation  $t$ -map and activation  $t$ -map will agree.

Our method is free from the above-mentioned problems. Namely, our method can sensitively detect the spatio-temporal emergence of activations through the investigation of the dynamic state transition and statistical evaluation across the repetition of the measurement. The earliest activation is localized in RVLM (the caudal part of pFRG), which can be seen typically with data2 (Fig. 6(c) in the time frame at -0.26 s). The activation extends bidirectionally to the rostral part of pFRG and to the preBötC region and travels to the high cervical spinal cord (Fig. 5(c) in the time frame at 0.64s, and Fig. 6(c) in the time frame at 0.26s).

We conclude that our method can precisely detect the biological activation without employing additional information such as reference time series data, and the significance can be evaluated with statistical test values. Further, it can be generally used to spatio-temporal data, e.g., functional magnetic resonance imaging (fMRI), electroencephalography (EEG), near infrared spectroscopy (NIRS).

#### REFERENCES

- [1] K. J. Friston, A. P. Holmes, K. J. Worsley, J. B. Poline, C. D. Frith, and R. S. J. Frackowiak, "Statistical parametric maps in functional imaging: A general linear approach," *Hum. Brain Mapp.*, vol. 2, no. 4, 1995, pp. 189-210.
- [2] Y. Oku, H. Masumiya, and Y. Okada, "Postnatal developmental changes in activation profiles of the respiratory neuronal network in the rat ventral medulla," *J. Physiol.*, vol. 585, no. 1, 2007, pp. 175-186.
- [3] Y. Oku, N. Kimura, H. Masumiya, and Y. Okada, "Spatiotemporal organization of frog respiratory neurons visualized on the ventral medullary surface," *Respir. Physiol. Neurobiol.*, vol. 161, no. 3, 2008, pp. 281-290.
- [4] Y. Okada, H. Masumiya, Y. Tamura, and Y. Oku, "Respiratory and metabolic acidosis differentially affect the respiratory neuronal network in the ventral medulla of neonatal rats," *Eur. J. Neurosci.*, vol. 26, no. 10, 2007, pp. 2834-2843.
- [5] T. Kailath, "An innovation approach to least-square estimation Part I: Linear filtering in additive white noise," *IEEE Trans. Automat. Contr.*, vol. AC-13, no. 6, 1968, pp. 646-655.
- [6] T. Kailath, "An innovation approach to least-square estimation Part II: Linear smoothing in additive noise," *IEEE Trans. Automat. Contr.*, vol. AC-13, no. 6, 1968, pp. 655-660.
- [7] H. Kato, and T. Ozaki, "Adding data process feedback to the nonlinear autoregressive model," *Signal Process.*, vol. 82, no. 9, 2002, pp. 1189-1204.
- [8] J. C. Jimenez and T. Ozaki, "An approximate innovation method for the estimation of diffusion processes from discrete data," *J. Time Ser. Anal.*, vol. 27, no. 1, 2006, pp. 77-97.
- [9] A. Galka, T. Ozaki, J. B. Bayard, and O. Yamashita, "Whitening as a tool for estimating mutual information in spatiotemporal data sets," *J. Stat. Phys.*, vol. 124, no. 5, 2006, pp. 1275-1315.
- [10] F. Miwakeichi, Y. Oku, Y. Okada, S. Kawai, Y. Tamura, M. Ishiguro, "Detection and visualization method of dynamic state transition for biological spatio-temporal imaging data", *IEEE Trans. Med. Imaging*, 30(3), 2011, pp. 859-66.
- [11] F. Miwakeichi, Y. Oku, Y. Okada, S. Kawai, Y. Tamura, M. Ishiguro, "A Spatio-temporal Filtering Method Based on an AR Type Model for Analysis of Single-trial Biological Imaging Data (in Japanese)", *Proceedings of the Institute of Statistical Mathematics*, 60-1, 2012, pp. 149-157.
- [12] G. E. P. Box, G. M. Jenkins, G. C. Reinsel, "Time Series Analysis (Fourth edition)", 2008, WILEY.
- [13] H. Akaike, "A new look at the statistical model identification", *IEEE Trans. Automat. Contr.*, AC-19, No. 6, 1974, pp. 716-723.
- [14] H. Onimaru and I. Homma, "A novel functional neuron group for respiratory rhythm generation in the ventral medulla", *J. Neurosci.*, vol. 23, no. 4, 2003, pp.1478-1486.
- [15] H. Onimaru, A. Arata, and I. Homma, "Primary respiratory rhythm generator in the medulla of brainstem-spinal cord preparation from newborn rat", *Brain Res.*, vol. 445, no.2, 1988, pp. 314-324.
- [16] J. C. Smith, H. H. Ellenberger, K. Ballanyi, D. W. Richter and J. L. Feldman, "Pre-Botzinger complex: a brainstem region that may generate respiratory rhythm in mammals", *Science*, vol. 254, no. 5032, 1991, pp. 726-729.